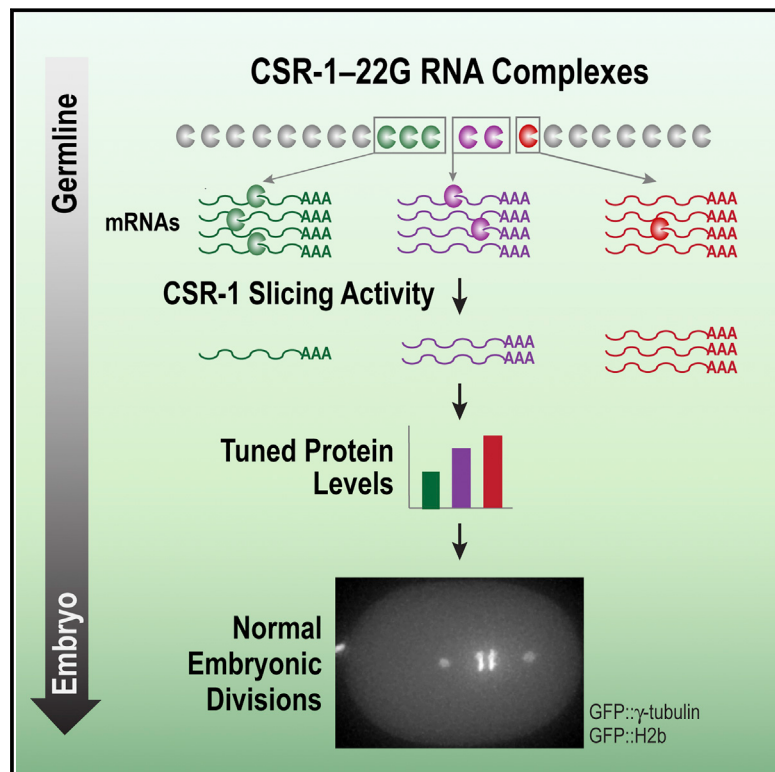


A Small RNA-Catalytic Argonaute Pathway Tunes Germline Transcript Levels to Ensure Embryonic Divisions

Graphical Abstract



Authors

Adina Gerson-Gurwitz, Shaohe Wang,
Shashank Sathe, Rebecca Green,
Gene W. Yeo, Karen Oegema,
Arshad Desai

Correspondence

abdesai@ucsd.edu

In Brief

The Argonaute CSR-1 employs its slicer activity to tune the transcript levels of its targets guided by the density of small RNA co-factors. CSR-1-mediated transcript tuning, rather than silencing, is essential to produce maternally loaded oocytes capable of supporting early embryogenesis.

Highlights

- Catalytic activity of the Argonaute CSR-1 is essential for early embryogenesis
- CSR-1 controls microtubule assembly by restricting expression of a depolymerase
- CSR-1 tunes germline transcript levels guided by density of small RNA cofactors

Accession Numbers

GSE75128

A Small RNA-Catalytic Argonaute Pathway Tunes Germline Transcript Levels to Ensure Embryonic Divisions

Adina Gerson-Gurwitz,^{1,2} Shaohe Wang,^{1,2,3} Shashank Sathe,^{2,4} Rebecca Green,^{1,2} Gene W. Yeo,^{2,3,4} Karen Oegema,^{1,2,3} and Arshad Desai^{1,2,3,*}

¹Ludwig Institute for Cancer Research, San Diego, CA 92093, USA

²Department of Cellular & Molecular Medicine, University of California San Diego, La Jolla, CA 92093, USA

³Biomedical Sciences Graduate Program, University of California San Diego, La Jolla, CA 92093, USA

⁴UCSD Stem Cell Program & Sanford Consortium for Regenerative Medicine, Institute for Genomic Medicine, La Jolla, CA 92093, USA

*Correspondence: abdesai@ucsd.edu

<http://dx.doi.org/10.1016/j.cell.2016.02.040>

SUMMARY

Multiple division cycles without growth are a characteristic feature of early embryogenesis. The female germline loads proteins and RNAs into oocytes to support these divisions, which lack many quality control mechanisms operating in somatic cells undergoing growth. Here, we describe a small RNA-Argonaute pathway that ensures early embryonic divisions in *C. elegans* by employing catalytic slicing activity to broadly tune, instead of silence, germline gene expression. Misregulation of one target, a kinesin-13 microtubule depolymerase, underlies a major phenotype associated with pathway loss. Tuning of target transcript levels is guided by the density of homologous small RNAs, whose generation must ultimately be related to target sequence. Thus, the tuning action of a small RNA-catalytic Argonaute pathway generates oocytes capable of supporting embryogenesis. We speculate that the specialized nature of germline chromatin led to the emergence of small RNA-catalytic Argonaute pathways in the female germline as a post-transcriptional control layer to optimize oocyte composition.

INTRODUCTION

Maternal loading of proteins and RNAs into oocytes by the female germline limits the requirement for transcriptional and translational activity during early embryogenesis. While the benefits of such a strategy are evident, it raises the question of how the composition of the maternal load is specified since homeostatic mechanisms that operate during growth may no longer be relevant. Thus, specific mechanisms are likely to exist in the female germline to ensure accurate stoichiometry of maternally loaded components. In the process of investigating a small RNA-Argonaute pathway previously implicated in chromosome segregation, we uncovered a mechanism that performs such a function in *Caenorhabditis elegans*.

Argonautes are a conserved class of proteins implicated in diverse small RNA-based processes (Carmell et al., 2002; Kuhn and Joshua-Tor, 2013; Swarts et al., 2014). Argonautes are particularly prominent in *C. elegans* (Billi et al., 2014; Grishok, 2013), where they have been implicated in diverse processes, including RNA interference (Tabara et al., 1999), transposon silencing (Batista et al., 2008; Das et al., 2008), self-/non-self-discrimination (Ashe et al., 2012; Gu et al., 2009; Lee et al., 2012; Seth et al., 2013; Shirayama et al., 2012), germline immortality (Buckley et al., 2012; Yigit et al., 2006), and transgenerational epigenetic inheritance (Ashe et al., 2012; Buckley et al., 2012; Shirayama et al., 2012). Of the 27 *C. elegans* Argonautes (Yigit et al., 2006), only one—CSR-1—is absolutely essential for fertility and embryo viability (Claycomb et al., 2009; Yigit et al., 2006). CSR-1 is bound to a class of small 22-nt RNAs with a guanosine on their 5' ends known as 22G RNAs (Gu et al., 2009). 22G RNAs act in two different Argonaute pathways in the germline, one employing CSR-1 and a second employing WAGO class Argonautes (Claycomb et al., 2009; Gu et al., 2009). CSR-1-bound 22G RNAs are homologous to germline-expressed transcripts, and CSR-1-22G RNA complexes have been suggested to act in a diverse array of processes: chromosome and centromere organization (Claycomb et al., 2009), maturation of core histone mRNAs (Avgousti et al., 2012), assembly of germline ribonucleoprotein structures known as P granules (Claycomb et al., 2009; Updike and Strome, 2009), protection of germline transcription via an effect on chromatin (Wedeles et al., 2013), definition of self versus non-self in a balance with the WAGO-22G RNA pathway that acts downstream of the Piwi class Argonaute PRG-1 and its associated 21U RNAs (Seth et al., 2013), promotion of sense transcription (Cecere et al., 2014), and translational control in the mitotic zone of the germline (Friend et al., 2012). A fundamental assumption in prior studies has been that CSR-1 does not significantly control transcript levels of target genes with homology to its bound 22G RNAs. This assumption, based on microarray analysis of *csr-1* mutants (Claycomb et al., 2009) and sequencing analysis following feeding RNAi-based reduction of CSR-1 (Campbell and Updike, 2015), is surprising because CSR-1 has conserved residues implicated in slicing (Yigit et al., 2006) and is required for the major slicing activity in *C. elegans* extracts (Aoki et al., 2007).

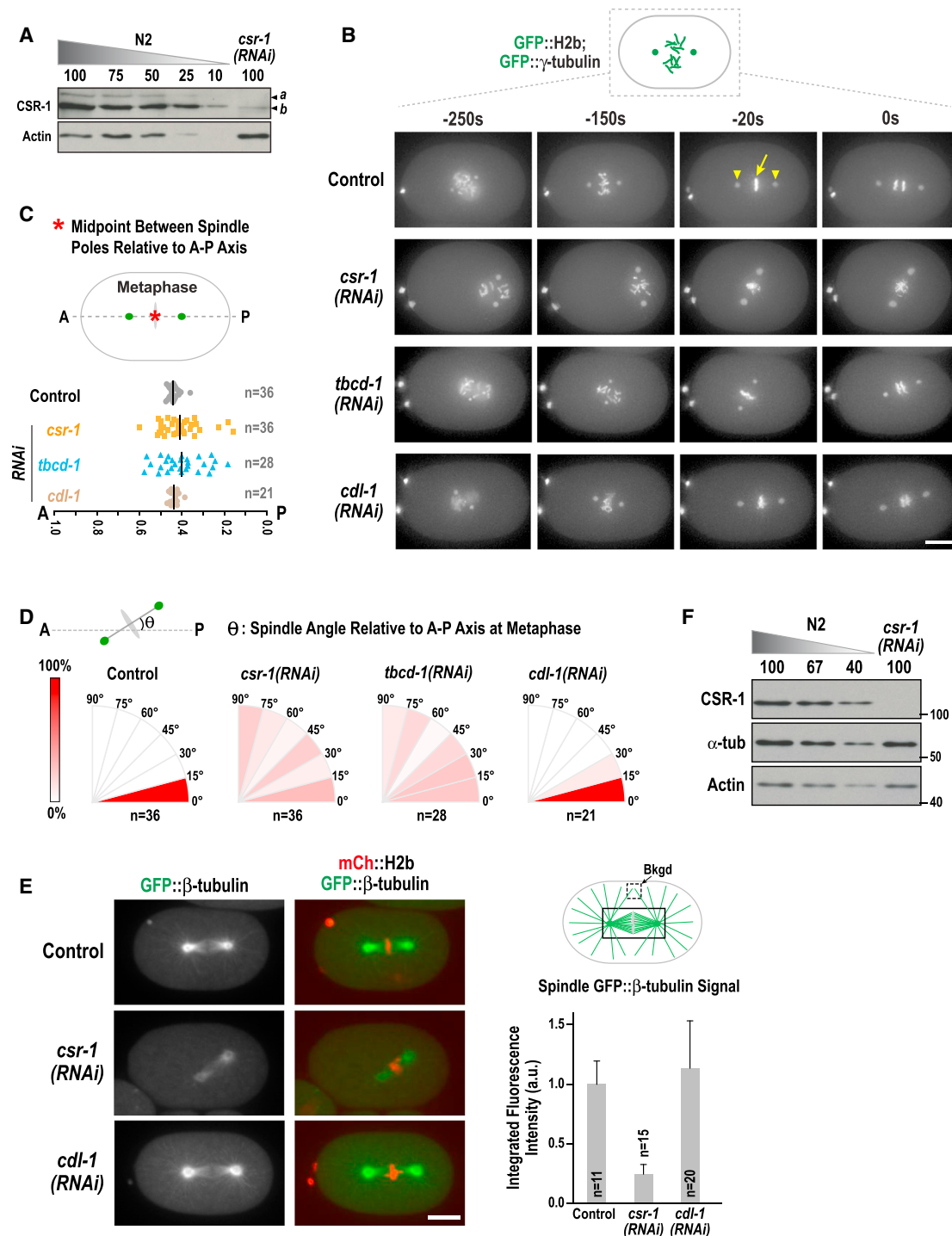


Figure 1. CSR-1 Inhibition Reduces Microtubule Assembly in One-Cell Embryos

(A) Immunoblot comparing a standard curve of N2 wild-type worm extract to CSR-1-depleted worm extract. β -actin serves as a loading control. Bands corresponding to the two CSR-1 isoforms (a and b; Figures S1A–S1C) are indicated.

(B) Images from time-lapse sequences of embryos expressing GFP::H2b (yellow arrow in control –20 s) and GFP:: γ -tubulin (yellow arrowheads in control –20 s) for the indicated conditions. Time is in seconds relative to early anaphase. Scale bar, 10 μ m.

(C) Plot of the position of the spindle midpoint (defined in maximal intensity projections as the midpoint between GFP:: γ -tubulin foci) projected onto the embryo A-P axis at metaphase for the indicated conditions.

(D) Plot of the distribution of the minimum angle between the spindle axis (defined in maximal intensity projections by a line connecting the GFP:: γ -tubulin foci) and the embryo A-P axis at metaphase for the indicated conditions.

(legend continued on next page)

In prior work, we found that genes with homology to CSR-1-bound 22G RNAs are in genomic regions depleted of the centromere-specific histone H3 variant CENP-A (Gassmann et al., 2012), raising the possibility that CSR-1-22G RNA complexes limit centromeric domains on holocentric *C. elegans* chromosomes. This, together with the chromosome segregation defect observed in early *C. elegans* embryos, prompted us to investigate how CSR-1 contributes to chromosome segregation. Using high-resolution phenotyping in early embryos to compare the effects of removing CSR-1 to selective ablation of its catalytic slicing activity, we found that loss of slicing activity fully phenocopied CSR-1 removal. In addition, while chromosome and centromere organization were unaffected, CSR-1 inhibition resulted in severe defects in the microtubule cytoskeleton caused by elevated expression of a kinesin-13 microtubule depolymerase prominently represented in the ensemble of CSR-1-22G RNA complexes. Genome-wide analysis revealed widespread 22G RNA density-dependent tuning, but not silencing, of target gene expression by CSR-1 slicing activity. Thus, CSR-1 slicing activity, guided by bound 22G RNAs, tunes the expression of a large number of germline-encoded transcripts to generate a balanced maternal load that can support embryogenesis.

RESULTS

CSR-1 Inhibition Reduces Microtubule Assembly in One-Cell Embryos

To dissect the role of CSR-1 in chromosome segregation, we analyzed the consequences of removing CSR-1 on the first embryonic cell division. As CSR-1 has been proposed to act with CDL-1, which binds the 3' UTR of core histone mRNAs to promote their maturation and translation (Avgousti et al., 2012), we also analyzed CDL-1 depletion in parallel. CSR-1 has a short isoform *b* and a longer isoform *a*. CSR-1*b* is functionally critical in embryos as depleting isoform *a* alone did not affect embryonic viability, whereas depleting >95% of both isoforms led to penetrant embryonic lethality (Figures 1A and S1A–S1C).

Filming one-cell embryos co-expressing GFP::histone H2b and GFP:: γ -tubulin, which label the chromosomes and spindle poles, respectively, revealed a clear difference in the CSR-1 and CDL-1 depletion phenotypes (Figure 1B). CSR-1 depletion led to phenotypes characteristic of defects in the microtubule cytoskeleton, including unstable positioning of the mitotic spindle along the A-P axis (Figures 1B and 1C) and randomization of metaphase spindle angle relative to the A-P axis (Figures 1B and 1D). These phenotypes were similar to those following depletion of the tubulin chaperone TBCD-1 (Figures 1B–1D; tubulin-specific cofactor D). CDL-1 depletions, which reduced global histone levels (Figure S1D; Avgousti et al., 2012), did not exhibit these phenotypes but instead exhibited defects in chromosome condensation and structure (Figure 1B, ~250 s; Figure 2A, below). Imaging in a strain expressing GFP:: β -tubulin

and mCherry::H2b revealed greatly reduced microtubule assembly in CSR-1 and TBCD-1, but not in CDL-1-depleted embryos (Figure 1E and S1H). α -tubulin levels were not changed by CSR-1 depletion (Figure 1F), suggesting that the reduction in microtubule assembly is not due to reduced availability of α/β -tubulin dimers.

CSR-1 binds 22G RNAs generated by the EGO-1/DRH-3/EKL-1 complex (Gu et al., 2009). Imaging embryos depleted of EGO-1, DRH-3, or EKL-1 revealed phenotypes similar to CSR-1 depletion, indicating that the contribution of CSR-1 to microtubule assembly depends on its association with 22G RNAs (Figures S1E–S1G). We conclude that whereas CDL-1 inhibition results in defects in chromatin structure consistent with its proposed role in histone production, inhibition of CSR-1 or the factors that generate its bound 22G RNAs leads to a severe defect in microtubule assembly.

CSR-1 Inhibition Does Not Affect Chromosome Structure or Centromere/Kinetochore Assembly in One-Cell Embryos

CSR-1-22G RNA complexes have been proposed to control chromosome architecture and centromere organization in the early embryo, potentially by controlling histone mRNA processing and/or by guiding deposition of the centromeric histone variant CENP-A (Avgousti et al., 2012; Claycomb et al., 2009). Our initial analysis suggested that CSR-1 depletion did not cause visible defects in mitotic chromosome structure. Consistent with this impression, closer analysis revealed that while CDL-1 depletion caused chromosome condensation defects during mitotic entry, chromosomes were normally condensed in CSR-1-depleted embryos (Figure 2A). Both CSR-1 and CDL-1 depletion led to lagging anaphase chromatin; however, the morphology was distinct (Figure 2A). In CSR-1-depleted embryos, condensed chromosomes were lagging, whereas in CDL-1-depleted embryos, poorly condensed chromatin was stretched between the separating chromosome masses. We conclude that the segregation defects in CSR-1-depleted embryos cannot be explained by action in the CDL-1-dependent histone mRNA maturation pathway.

To test the proposal that CSR-1 patterns centromere/kinetochore architecture (Claycomb et al., 2009; Gassmann et al., 2012), we analyzed a functional GFP fusion with the centromeric histone variant CENP-A^{HCP-3}, which forms the structural foundation for kinetochore assembly (Figure 2B). GFP::CENP-A^{HCP-3} was patterned into two stripes that ran along the length of the holocentric chromosomes in early prometaphase embryos (Figure 2C). Qualitative assessment and quantitative line scans across individual chromosomes revealed essentially identical localization in control and CSR-1-depleted embryos (Figure 2D). In contrast, CDL-1-depleted embryos exhibited abnormal GFP::CENP-A^{HCP-3} localization (Figure 2C), consistent with defective chromosome condensation (Figure 2A).

(E) Representative images (left) and quantification (right) of metaphase spindle GFP:: β -tubulin signal for the indicated conditions. Background-subtracted integrated fluorescence intensity measurements were normalized to the control mean value. Scale bar, 10 μ m.

(F) Immunoblot of α -tubulin in *csr-1(RNAi)* compared to a standard curve of N2 (control) worms. β -actin serves as a loading control. Molecular weight markers (in kilodaltons) are indicated on the right.

See also Figure S1 and Tables S2, S3, and S5.

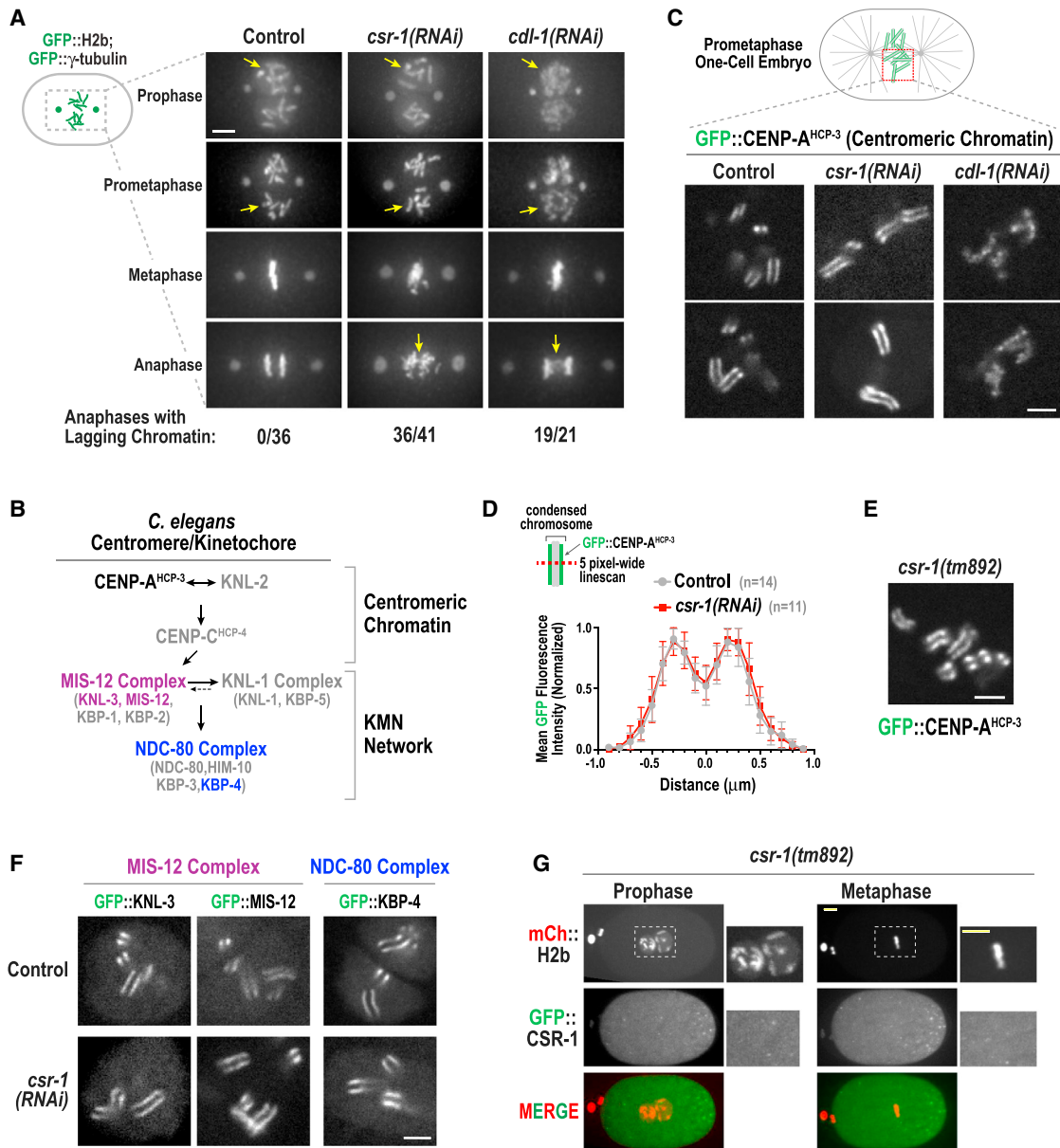


Figure 2. CSR-1 Inhibition Does Not Perturb Chromosome Structure or Centromere/Kinetochore Architecture in One-Cell Embryos

(A) Images from the nuclear region from time-lapse sequences of one-cell embryos expressing GFP:H2b and GFP: γ -tubulin. Arrows highlight features of the chromosome structure at different stages in control, *csr-1(RNAi)*, and *cdl-1(RNAi)* that are discussed in the text. Scale bar, 10 μ m.

(B) Schematic summary of *C. elegans* centromere/kinetochore assembly.

(C) Single-plane confocal images of GFP::CENP-A^{HCP-3} for the indicated conditions. Two examples are shown per condition. Scale bar, 5 μ m.

(D) Line scan analysis of GFP::CENP-A^{HCP-3} fluorescence on condensed chromosomes. 5 pixel-wide individual line scans of single chromosomes were normalized based on peak intensity, centered on the valley between the peaks of GFP signal, and averaged. Error bars represent SD. Control, n = 14 chromosomes from six embryos. *csr-1(RNAi)*, n = 11 chromosomes from nine embryos.

(E) Single-plane confocal image of GFP::CENP-A^{HCP-3} in a rare one-cell embryo derived from a *csr-1(tm892)* homozygous worm. Scale bar, 5 μ m.

(F) Single-plane confocal images for the indicated GFP-fused kinetochore components. See also Figure S2B. Scale bar, 5 μ m.

(G) Maximum intensity z stack projections of prometaphase and metaphase stage one-cell *csr-1(tm892)* embryos rescued by expression of GFP::CSR-1 from a single-copy transgene (Figures S2C–S2E). The embryos also express mCherry::H2b. The magnified images of boxed regions are shown on the right. Scale bars, 5 μ m. See also Figure S2 and Tables S2 and S3.

These results were confirmed by analysis of rare one-cell embryos from the *csr-1(tm892)* null mutant, which has severely reduced fertility (Figures 2E and S2A), and by analysis of three

outer kinetochore components (Figure 2B; Cheeseman et al., 2004): KNL-3, MIS-12, and KBP-4 (Figures 2F and S2B). Thus, CSR-1 depletion does not lead to detectable alterations in

centromere/kinetochore architecture at the resolution of light microscopy.

In strains in which the sole source of CSR-1 was GFP::CSR-1 encoded by a functional single-copy transgene (Figures S2C and S2D), we observed the previously described P-granule localization (Figure S2E) but no detectable GFP signal on chromosomes in oocytes (Figure S2E) or early mitotic embryos (Figure 2G). Thus, there is not a substantial population of CSR-1-22G RNA complexes enriched on mitotic chromatin. We conclude that CSR-1 inhibition leads to greatly reduced microtubule assembly, but not to detectable defects in chromosome or centromere/kinetochore structure.

CSR-1 Slicing Activity Is Required for Its Function in Embryos and in the Germline

To investigate the function of CSR-1 slicing activity, we generated single-copy untagged RNAi-resistant transgenes encoding WT CSR-1 and a Slicing Inactive (SIN) mutant in which the aspartate active-site residues of slicing Argonautes (D606, D681 in CSR-1b; Aoki et al., 2007; Yigit et al., 2006) were mutated to alanines (Figures 3A and S3A). Whereas transgene-encoded CSR-1^{WT} rescued the lethality associated with depletion of endogenous CSR-1, CSR-1^{SIN} did not (Figure 3B). The same result was obtained by crossing the transgenes into the *csr-1(tm892)* mutant (data not shown). CSR-1^{WT}, in a homozygous *csr-1(tm892)* background, was expressed at a level similar to endogenous CSR-1 in control N2 worms (Figure 3C). In contrast, despite expression from a single copy targeted transgene with an identical promoter and 5' and 3' UTR regions, CSR-1^{SIN} was overexpressed (Figures 3C and S3B), suggesting that CSR-1 slicing autoregulates its own expression (see below). The one-cell embryo phenotypes in the presence of CSR-1^{SIN}, including a severe reduction in microtubule assembly, were essentially identical to those observed following CSR-1 depletion (Figures 3D–3G and S3C). We conclude that the early embryonic functions of CSR-1 depend on its slicing activity.

Mutational inactivation of *csr-1* leads to a significant reduction in brood size (Figures 3H and S2D), and the germlines of both *csr-1(tm892)* null and *csr-1^{SIN};csr-1(tm892)* slicing activity mutant worms exhibited increased apoptotic figures and multinucleation (Figure S3D). Interestingly, *csr-1^{SIN};csr-1(tm892)* worms laid ~2-fold more embryos than *csr-1(tm892)* worms, suggesting a potential slicing activity-independent contribution of CSR-1 to embryo production. Like CSR-1^{WT}, a GFP fusion with CSR-1^{SIN} still localized to perinuclear P granules in the germline of L4 larvae (Figure S3E); in adult worms, the overexpressed CSR-1^{SIN} slicing mutant formed aggregates in addition to perinuclear granules (data not shown). We conclude that CSR-1 catalytic activity is important for embryonic divisions and for normal germline function.

CSR-1 Slicing Activity Restricts Expression of the Microtubule Depolymerase MCAK^{KLP-7}

The embryonic phenotypes resulting from selective ablation of CSR-1 slicing activity suggest that CSR-1 slicing activity controls expression of a target or set of targets that regulate microtubule assembly. Examination of prior sequencing data (Claycomb et al., 2009) to identify genes encoding microtubule

regulators with homology to CSR-1-bound 22G RNAs revealed that *klp-7*, the gene encoding the sole MCAK-related kinesin-13 in *C. elegans*, was ranked fifth out of 4,191 genes with >25 normalized reads; *csr-1* itself was ranked 15th (Figure S4A). MCAK^{KLP-7} is a non-motile kinesin that acts as a potent microtubule-depolymerizing enzyme, triggering growing microtubules to transition from polymerization to depolymerization (Figure 4A; Desai et al., 1999). To determine whether increased MCAK^{KLP-7} expression was responsible for the reduced microtubule assembly in embryos lacking CSR-1 slicing activity, we first measured *klp-7* and *csr-1* mRNA levels by RT-qPCR and followed that with quantitative immunoblotting (performed as described in Figure S4B). Since levels of MCAK^{KLP-7} in N2 and *csr-1^{WT};csr-1(tm892)* were equivalent (Figure S4C), as also shown for CSR-1 (Figure 3C), we employed a balanced heterozygous *csr-1(tm892)* mutant strain homozygous for the *csr-1^{SIN}* transgene, picked equal number of first generation homozygous *csr-1^{SIN};csr-1(tm892)* or control N2 worms, and isolated RNA or prepared extracts for immunoblotting. Both *klp-7* and *csr-1* mRNAs were significantly elevated in the *csr-1^{SIN};csr-1(tm892)* mutant (Figure 4B), indicating that CSR-1 slicing activity suppresses their levels. Immunoblotting of whole-worm extracts revealed consistent ~3.5- and 3-fold elevation of MCAK^{KLP-7} and CSR-1^{SIN} protein levels, respectively (Figures 4C and S3B). Equivalent elevation of MCAK^{KLP-7} was also observed following CSR-1 depletion (Figure 4C).

To determine if the 3.5-fold elevation of MCAK^{KLP-7} protein accounted for the reduced microtubule assembly in CSR-1-depleted embryos, we employed a 1:16 ratio of double-stranded RNAs (dsRNAs) targeting MCAK^{KLP-7} and CSR-1 to reduce MCAK^{KLP-7} to 0.35- to 0.5-fold of wild-type (WT) levels, while maintaining CSR-1 depletion (Figure 4D). Eliminating MCAK^{KLP-7} elevation rescued the microtubule assembly defect in CSR-1-depleted one-cell embryos (Figure 4E), indicating that MCAK^{KLP-7} elevation accounts for this prominent defect associated with loss of CSR-1 function. However, reduction of MCAK^{KLP-7} did not rescue the chromosome missegregation in CSR-1-depleted embryos (Figure 4F) or restore embryonic viability (data not shown), indicating it is not the sole CSR-1 target whose overexpression leads to embryonic division defects. Examination of a strain expressing a functional fusion with GFP integrated just before the stop codon at the endogenous *klp-7* locus revealed that CSR-1 depletion led to the significant elevation of MCAK^{KLP-7}::GFP fluorescence in the germline (Figure 4G). This result suggests that excess maternally loaded MCAK^{KLP-7} underlies the severe microtubule assembly defect in CSR-1-depleted and CSR-1 slicing activity mutant embryos.

CSR-1 Slicing Activity Controls Protein Levels of a Number of Components Implicated in Embryonic Cell Divisions

While elevated MCAK^{KLP-7} expression accounts for the microtubule assembly defect in CSR-1-inhibited one-cell embryos, other targets are also likely misregulated. To begin to assess the scope of CSR-1 slicing activity-mediated regulation, we employed 44 validated antibodies against *C. elegans* proteins important for embryonic cell division and/or germline function

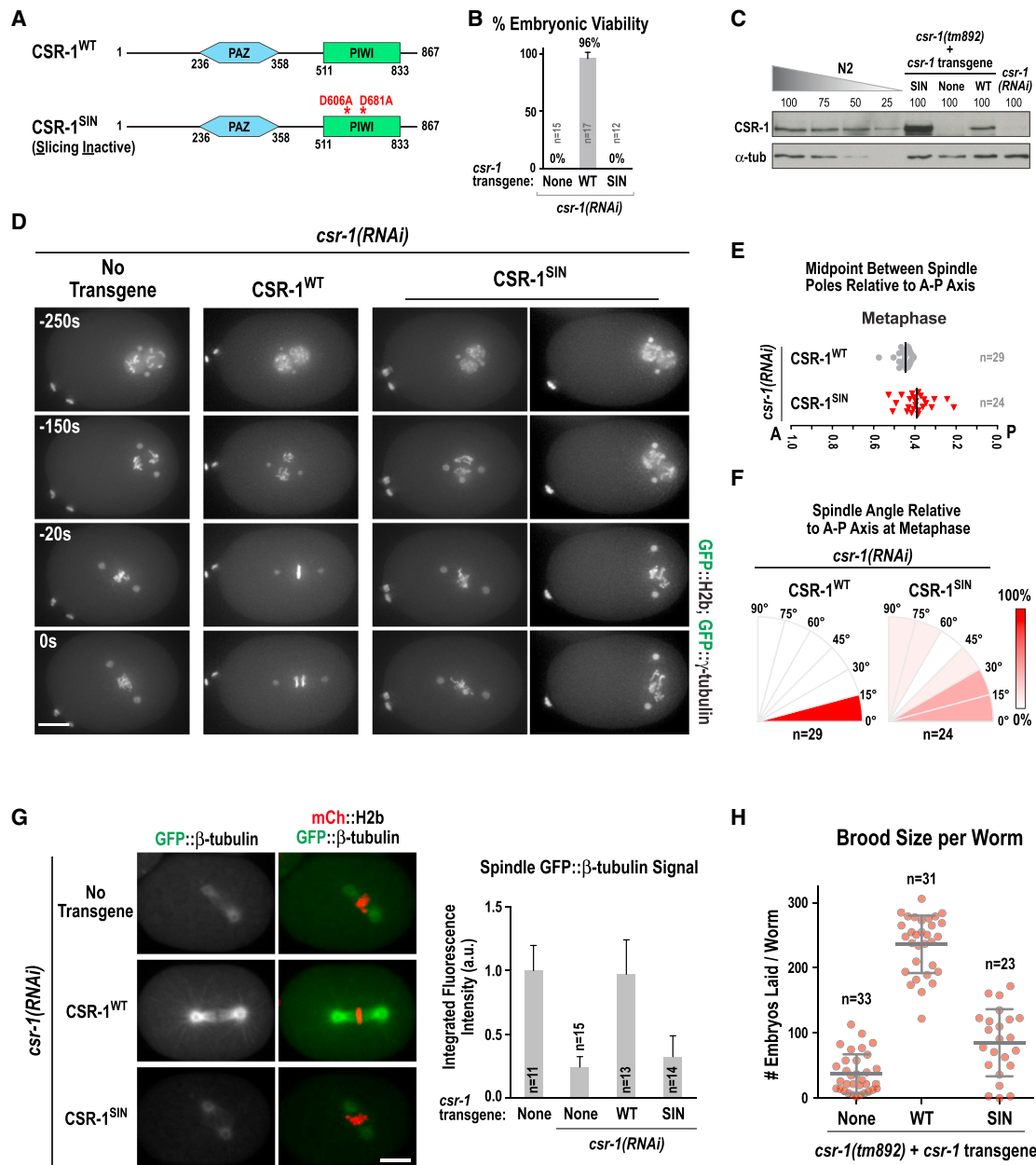


Figure 3. Selective Mutation of CSR-1 Slicing Activity Phenocopies CSR-1 Depletion in One-Cell Embryos

- (A) Schematics of WT and slicing-inactive (SIN) CSR-1 expressed from targeted single-copy RNAi-resistant transgene insertions (see Figure S3A). The amino acid numbering is for the CSR-1b isoform, which is essential for embryogenesis.
- (B) Analysis of embryo viability for the indicated conditions. *n* is the number of worms analyzed; >977 progeny embryos were scored per condition. Error bars represent SD.
- (C) Immunoblotting of CSR-1 in the indicated conditions. The numbers above the lanes indicate percent loading, based on number of worms. α -tubulin served as a loading control.
- (D) Images from time-lapse sequences of one-cell embryos expressing GFP:H2b and GFP:: γ -tubulin, for the indicated conditions. Time is in seconds relative to anaphase. Scale bar, 10 μ m.
- (E) Spindle positioning relative to the embryo A-P axis, measured at metaphase as in Figure 1C, for the indicated conditions.
- (F) Spindle angle relative to the embryo A-P axis at metaphase, measured as in Figure 1D, for the indicated conditions.
- (G) Representative images (left) and quantification (right) of metaphase spindle GFP:: β -tubulin signal for the indicated conditions, measured as in Figure 1E. Error bars represent SD. Scale bar, 10 μ m.
- (H) Brood size per worm measured for first generation *csr-1(tm892)* homozygous worms, derived from balanced heterozygous mothers. When present, single-copy insertion *csr-1* transgenes were already homozygous in the balanced mothers.

See also Figure S3 and Tables S2, S3, and S25.

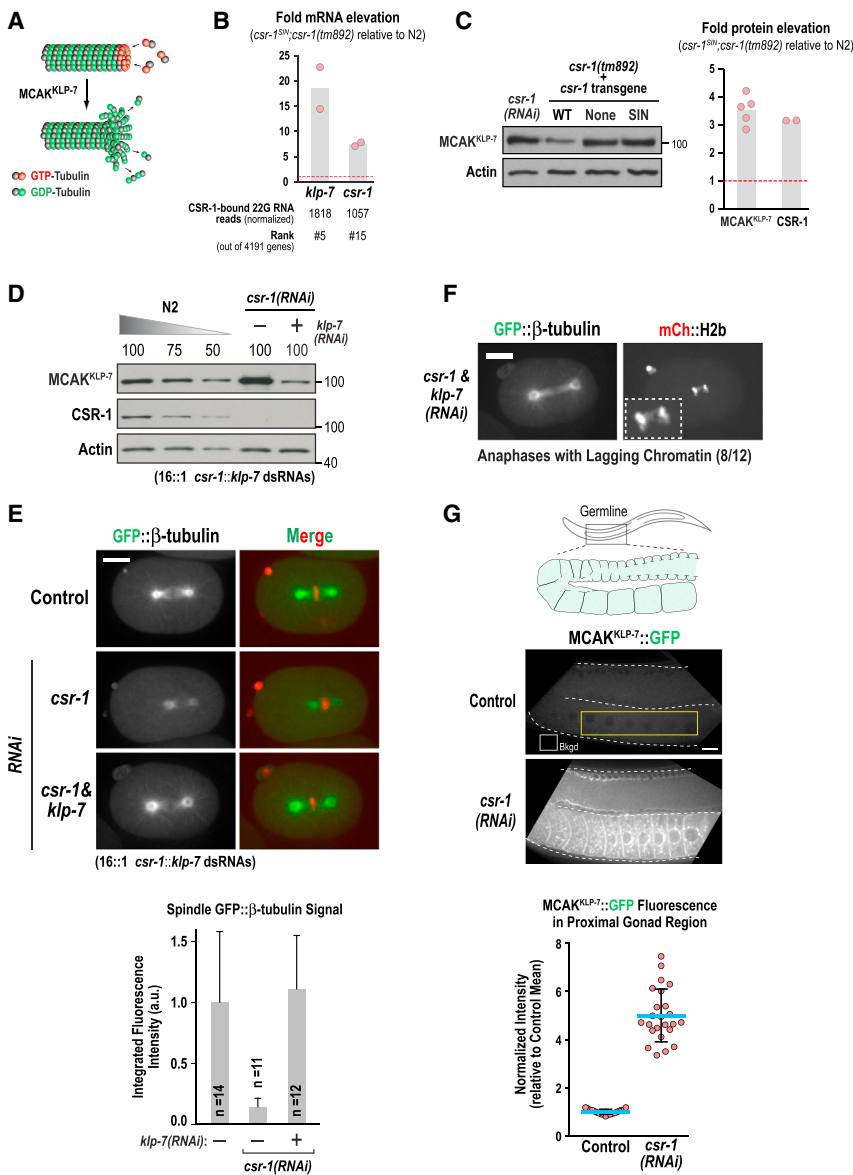


Figure 4. MCAK^{KLP-7} Overexpression Underlies the Reduced Microtubule Assembly in CSR-1-Inhibited One-Cell Embryos

(A) Schematic of MCAK^{KLP-7} activity. MCAK^{KLP-7} promotes microtubule disassembly by triggering the transition from polymerization to depolymerization.

(B) Comparison of mRNA levels in *csr-1*^{SIN}; *csr-1*(*tm892*) worms to N2 wild-type worms for the indicated genes; actin mRNA measured in parallel was used for normalization. Three replicates were analyzed per gene; the SD of replicate values was <1%, and their average is plotted from two experiments (light red dots; the gray bar is the mean of the two experiments). The red dashed line indicates no change in mRNA levels.

(C) Immunoblot analysis of MCAK^{KLP-7} and CSR-1 for the indicated conditions. The graph on the right plots the measurement of protein levels by immunoblotting normalized relative to β-actin. Each dot represents an independent measurement. The red dashed line indicates no change in protein levels.

(D and E) Co-depletion of CSR-1 and MCAK^{KLP-7}, analyzed by immunoblotting (D) and imaging of GFP::β-tubulin (E). A mixture with a 1:16 ratio of dsRNAs targeting *klp-7* and *csr-1* was employed in these experiments. Metaphase spindle GFP-β-tubulin signal was measured as in Figure 1E. Error bars represent SD. Scale bar, 10 μm.

(F) Images of an anaphase stage one-cell embryo co-depleted for CSR-1 and MCAK^{KLP-7}. Inset in the mCh::H2b channel shows lagging chromatin; frequency of lagging chromatin is indicated below the images. Scale bar, 10 μm.

(G) Images and quantification of endogenous locus-tagged MCAK^{KLP-7}::GFP in the proximal region of the germline. A region outside the worm was used for background subtraction (box marked “bkgd”). A fixed size box (yellow outline; 360 × 70 pixels) was drawn in the proximal germline region of imaged worms to measure MCAK^{KLP-7}::GFP fluorescence. Background-subtracted fluorescence intensity values, normalized to the control mean value, are plotted in the graph below. The blue lines mark the mean values; error bars represent SD. Scale bar, 10 μm.

See also Figure S4 and Tables S2, S3, S4, and S5.

(Figure 5A). The genes encoding all of these proteins have >25 normalized reads of homologous CSR-1-bound 22G RNAs (Claycomb et al., 2009). As a control, we monitored PTRN-1 (patriotin), a microtubule minus-end binding protein not expressed in the germline (Wang et al., 2015) that does not have homologous CSR-1-bound 22G RNAs. Protein levels in homozygous *csr-1*^{SIN}; *csr-1*(*tm892*) worm extract were compared to a standard curve for wild-type N2 worm extract on the same gel (Figure 5B); actin was used to normalize loading. Blots were quantified when the intensity of the test protein and loading controls in the *csr-1*^{SIN}; *csr-1*(*tm892*) lane fell within the N2 standard curve or required limited extrapolation (Figure S4B). The majority of target blots were repeated 2–5 times; while the results were consistent between repeats, the criteria for quantification were only met in the subset of experiments that are plotted. This analysis revealed elevated expression of 25 of the 44 targets in the

absence of CSR-1 slicing activity (Figures 5B and 5C; 19 [43%] targets >1.5-fold and 25 [57%] targets > PTRN-1). For the remaining targets, protein expression either did not change significantly (12 targets = 27%) or was decreased (<0.8-fold; 7 targets = 16%). To assess if reduced protein levels of specific targets reflected a positive role for CSR-1 slicing activity in transcription, we measured mRNA levels for six target genes—two of which exhibit elevated protein levels (*spd-1* and *spd-2*) and four of which exhibit reduced protein levels (*sgo-1*, *ani-1*, *npp-12*, and *gsp-1*)—as well as for the control *ptrn-1*. We did not observe reduced mRNA levels for any of the tested CSR-1 target genes (Figure 5D). Thus, the reduction in protein levels for some targets is not due to reduced transcript levels and may reflect a role for CSR-1 slicing activity in translation of specific mRNAs or be an indirect consequence of germline defects in *csr-1*^{SIN}; *csr-1*(*tm892*) worms (Figures 3H and S3D).

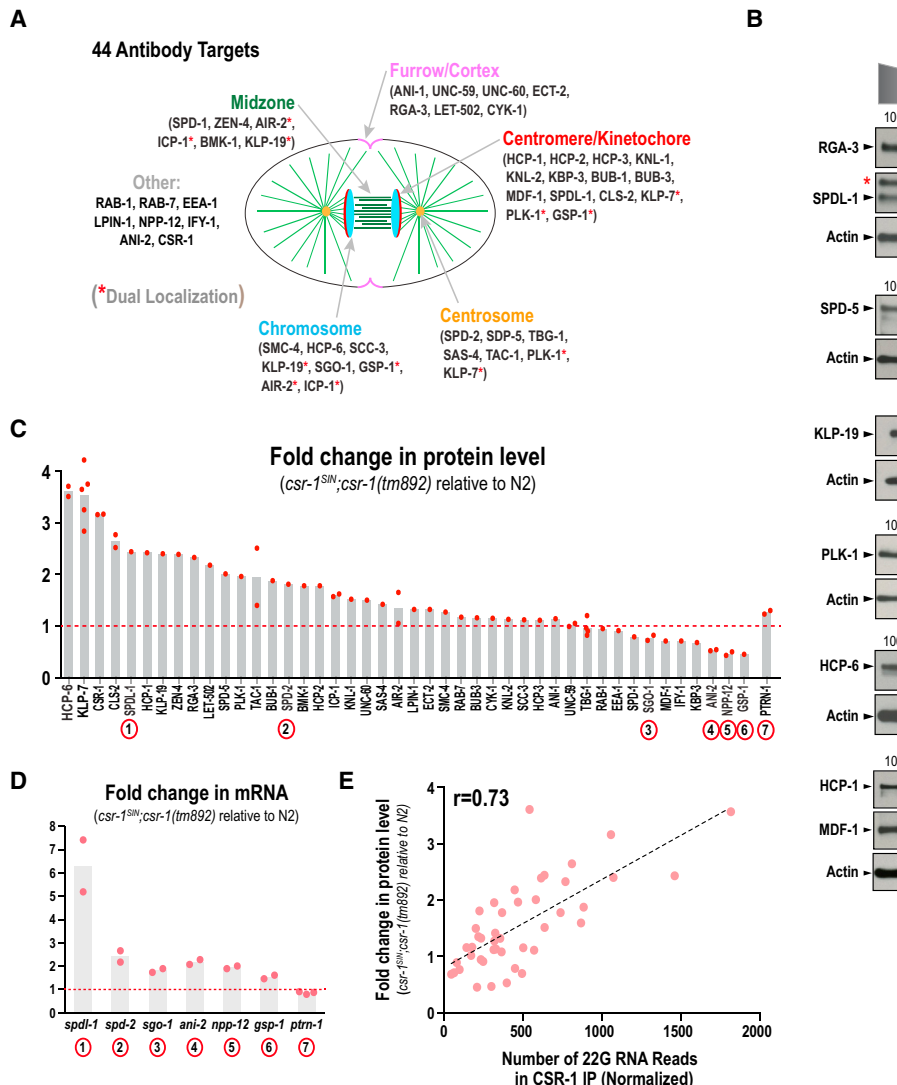


Figure 5. CSR-1 Slicing Activity Modulates Expression of Multiple Targets that Participate in Embryonic Cell Division

(A) Schematic of 44 targets employed for analysis of CSR-1 slicing activity-dependent changes in protein levels.

(B) Representative immunoblots comparing protein levels in the absence of CSR-1 slicing activity to a N2 wild-type standard curve. Actin serves as a loading control. The numbers above the lanes indicate percent loading, based on number of worms. The numbers above the test sample are shown in parentheses, as loading was calculated based on the actin standard curve (Figure S4B). A red asterisk indicates a background band.

(C) Plot of protein-level measurements for all targets, comparing *csr-1^{SIN}; csr-1(tm892)* worms to a standard curve of N2 wild-type. The light red dots represent individual measurements. The dashed red line marks no change in protein level.

(D) RT-qPCR analysis, as in Figure 4B, comparing mRNA levels in *csr-1^{SIN}; csr-1(tm892)* worms to N2 wild-type worms for the indicated genes (their corresponding gene products are marked with circled numbers on Figure 5C).

(E) Correlation plot of the change in the level of a target protein to the normalized read count of CSR-1-bound 22G RNAs that are homologous to its encoding locus (22G RNA read data are from Claycomb et al., 2009).

See also Figure S5 and Tables S2, S4, and S5.

The list of proteins whose expression was elevated ~2-fold in the absence of CSR-1 slicing activity included the centrosomal proteins SPD-2 and SPD-5 (Figures 5B and 5C). SPD-2 is the *C. elegans* homolog of the human pericentriolar material (PCM) protein Cep192 and SPD-5 is the major PCM scaffold protein in *C. elegans* (Hamill et al., 2002; Woodruff et al., 2015). Prior work has shown that centrosome size is component limited, with increased protein levels leading to increased centrosome

size (Decker et al., 2011). Consistent with this, we observed ~2-fold increase in centrosome size in *csr-1^{SIN}; csr-1(tm892)* mutant embryos (Figure S5), supporting the conclusion that an imbalance in the maternal load caused by loss of CSR-1 slicing activity has functional consequences in the early embryo.

Plotting the fold change in each target protein's level against the normalized reads of CSR-1-bound 22G RNAs homologous to the gene encoding that protein (from Claycomb et al., 2009)

revealed a correlation ($r = 0.73$) between the abundance of CSR-1-bound 22G RNAs and the effect of loss of CSR-1 slicing activity on target protein expression (Figure 5E). This correlation suggests that transcripts with greater numbers of homologous CSR-1-bound 22G RNAs are sliced to a greater extent by CSR-1 than those with fewer homologous CSR-1-bound 22G RNAs. Thus, analysis of protein levels suggests that CSR-1 slicing activity tunes down the expression of a significant proportion of its target genes and that the magnitude of the tuning correlates with the abundance of CSR-1-bound 22G RNAs.

CSR-1 Slicing Activity Tunes Target mRNAs in a Graded Fashion Dictated by 22G RNA Density

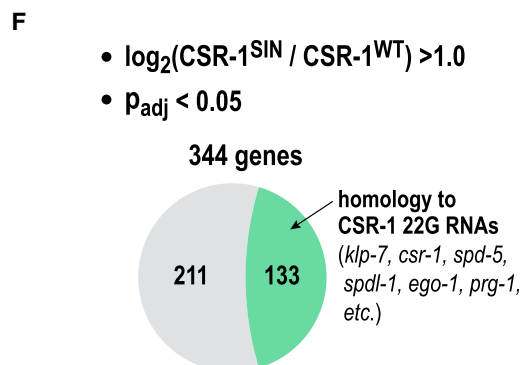
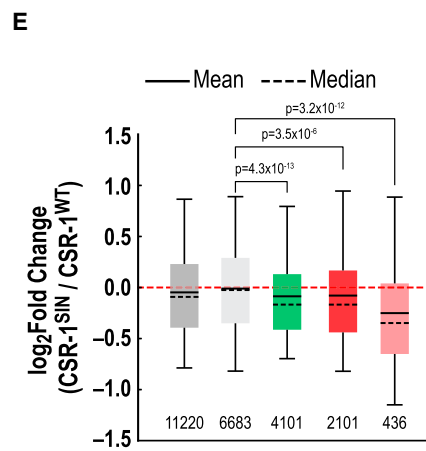
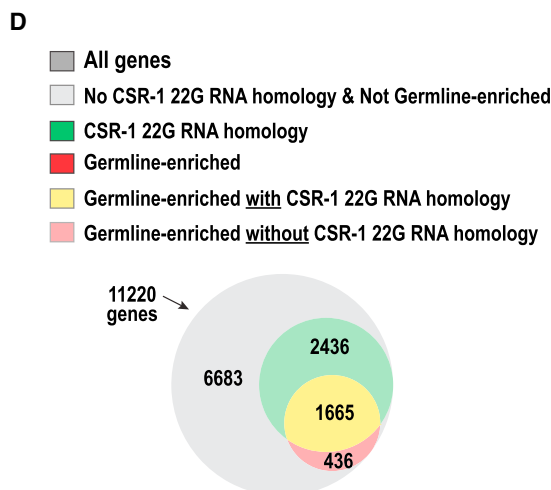
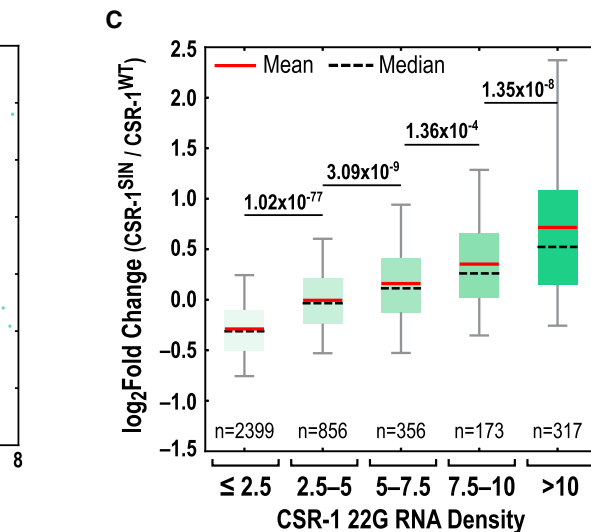
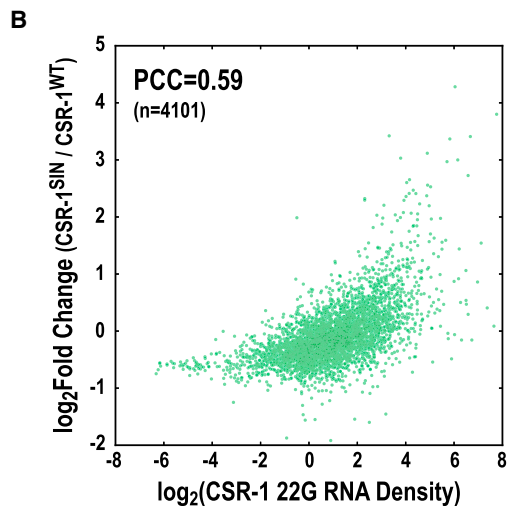
The phenotypic and immunoblotting analysis suggested that CSR-1 slicing activity is critical to generate a balanced maternal load capable of supporting early embryonic divisions. Since the immunoblotting analysis was restricted to proteins for which we had validated antibodies, we next performed mRNA Sequencing (mRNA-Seq) analysis to obtain an unbiased genome-wide view of the role of CSR-1 slicing activity in regulating target mRNA levels. We isolated mRNA from first-generation adult worms homozygous for the *csr-1* deletion and for transgenes encoding CSR-1^{WT} or CSR-1^{SIN}. N2 wild-type worms were picked in parallel, and two biological duplicates were processed for the three genotypes (Figures S6A and S6B). The CSR-1^{WT} mapped read profile was essentially identical to N2 (Figure S6B). With an expression threshold of RPKM >1 in N2 (RPKM, reads per kilobase of transcript per million reads) and a transcript size (defined as sum of annotated exons) >300 bp, we had 11,220 genes available for comparison between the CSR-1^{SIN} and CSR-1^{WT} datasets.

We were particularly interested in the effect of CSR-1 catalytic activity on the expression of genes with homology to CSR-1-bound 22G RNAs. 4,101 (97.9%) of the 4,191 genes with homology to CSR-1-bound 22G RNAs in N2 hermaphrodites (Claycomb et al., 2009) met the RPKM and transcript size thresholds (Figure 6A); 3,866 of these 4,101 genes (94%) are in the germline-expressed gene set defined by sequencing analysis of dissected gonads (Ortiz et al., 2014). Based on the correlation between the abundance of CSR-1-bound 22G RNAs and change in protein levels by immunoblotting (Figure 5E), we hypothesized that when CSR-1's catalytic activity is inhibited, the transcripts of genes that are more highly represented in the ensemble of CSR-1-22G RNA complexes increase to a greater degree than transcripts of genes with fewer corresponding CSR-1 22G RNAs. To test this prediction, we plotted the fold change in transcript level (CSR-1^{SIN}/CSR-1^{WT}) versus the "density" of 22G RNAs, which we defined as the ratio of CSR-1-bound 22G RNA reads to transcript abundance (RPKM) in N2 wild-type worms, for all 4,101 genes (Figure 6A). This analysis revealed a clear correlation between 22G RNA density and elevation of transcript levels in CSR-1^{SIN} versus CSR-1^{WT} (Figure 6B; Pearson correlation coefficient = 0.59). To visualize the positive correlation between increasing CSR-1 22G RNA density and the increase in transcript levels in CSR-1^{SIN} relative to CSR-1^{WT} in a different manner, we split the 4,101 gene set into five bins of increasing CSR-1 22G RNA density and plotted the change in transcript abundance between CSR-1^{SIN} and CSR-1^{WT} for the genes in each bin (Figures

6C and S6C). This analysis suggested graded tuning of transcript levels by CSR-1 slicing activity from low to high 22G RNA densities, rather than activity above a specific 22G RNA density threshold. We conclude that CSR-1 catalytic activity broadly tunes the transcript levels of genes with homologous CSR-1-bound 22G RNAs, with the amplitude of its tuning being dictated by 22G RNA density.

We noticed that the baseline when comparing transcript levels of the 4,101 genes with CSR-1 22G RNA homology between CSR-1^{SIN} and CSR-1^{WT} was lower than 1.0 (i.e., \log_2 foldchange < 0.0 at low 22G RNA densities; Figures 6B and 6C). Consistent with this, the distribution of fold change (CSR-1^{SIN}/CSR-1^{WT}) in transcript levels for the 4,101 genes with homology to CSR-1-bound 22G RNAs was slightly skewed to a negative value (median -0.17; mean -0.09; Figures 6D, 6E, and S6D). Since CSR-1-bound 22G RNAs are primarily homologous to germline-expressed genes, we wondered whether this mild negative skew reflected a direct effect or was an indirect consequence of the effect of inhibiting CSR-1 activity on germline architecture (Figures 3H and S3D). To distinguish between these possibilities, we analyzed 2,101 germline-enriched genes, defined by microarray-based comparison of a mutant that lacks a germline to control wild-type worms (Reinke et al., 2004). A majority (1,665/2,101) of the germline-enriched genes have homologous CSR-1 22G RNAs, while a small subset (436/2,101) lack CSR-1 22G RNA homology (Figure 6D); 90% of the 436 genes in this subset were confirmed to be germline expressed by RNA sequencing of isolated gonads (Ortiz et al., 2014). The germline-enriched gene subset without CSR-1 22G RNA homology also exhibited a negatively skewed fold-change distribution (median -0.35; mean -0.25; Figures 6E and S6D). Thus, the modest reduction in transcript levels for germline genes (both with and without homologous CSR-1-bound 22G RNAs) is potentially an indirect consequence of the effects of inhibiting CSR-1 slicing activity on germline architecture (Figures 3H and S3D).

Finally, we identified genes whose transcript levels increased most significantly between CSR-1^{SIN} and CSR-1^{WT} (>2-fold with adjusted p value < 0.05; we note that the germline architecture defects in CSR-1^{SIN} may make this an underestimate). This analysis revealed 344 genes, 133 of which were in the gene set defined by homology to CSR-1-bound 22G RNAs and included expected genes such as *klp-7*, *csr-1*, and *spd-5* (Table S1). Notably, 211 of the 344 genes whose transcript levels increased >2-fold did not have reported CSR-1-bound 22G RNAs (Table S1). A comparison of transcript abundance revealed that this 211 gene set is expressed at substantially lower levels compared to the 133 genes with homology to CSR-1-bound 22G RNAs (Figure S6E). Thus, it is possible that there are CSR-1-bound 22G RNAs homologous to these 211 genes that have not been detected/did not meet thresholds due to low abundance. 194 of these 211 genes (92%) were not germline-enriched (as defined by (Reinke et al., 2004) and 103 (49%) were absent from the most comprehensive germline-expressed gene set (Ortiz et al., 2014). Thus, if these are indeed CSR-1 regulated genes, a significant subset may be acting in non-germline contexts. Additional work will be necessary to test whether these genes are indeed CSR-1 catalytic activity-regulated and to assess the functional significance of their regulation.



(legend on next page)

DISCUSSION

CSR-1 is unique among the 27 *C. elegans* Argonautes in that its inhibition leads to immediate and severe embryonic division phenotypes. While prior studies have ascribed many potential roles to CSR-1, they have discounted slicing activity-dependent control of target expression. Here, by focusing on phenotypic signatures in the one-cell embryo, we show that CSR-1 function in embryonic cell division is entirely dependent on its slicing activity. This is consistent with biochemical data showing that CSR-1 provides the dominant slicing activity in *C. elegans* extracts (Aoki et al., 2007) and with increased mRNA levels for genes such as *klp-7* and *csr-1* in *ego-1* mutants, where 22G RNA production is inhibited (Maniar and Fire, 2011). Notably, many CSR-1 targets have essential functions; thus, CSR-1 slicing activity, guided by the small RNA biogenesis machinery, tunes, rather than silences, target expression (Figure 7). Below, we discuss the relationship of this finding to other proposed roles for CSR-1, the relevance of the mechanism described here to other species, and the potential reasons why small RNA-catalytic Argonaute pathways may have evolved to provide a post-transcriptional layer of regulation in the female germline.

Relationship of Tuning Activity to Previously Proposed Roles of CSR-1

An important question emerging from our work is the relationship of CSR-1 slicing activity-dependent target tuning to its other proposed functions. Given the misregulation of a substantial number of targets, the assumption in prior studies that CSR-1 does not significantly control target expression is not valid. The reasons for this discrepancy are not clear but may involve technical differences—in the initial study of *csr-1* mutants, microarrays were employed instead of sequencing (Claycomb et al., 2009); in a recent study employing sequencing (Campbell and Updike, 2015), CSR-1 was depleted by feeding-based RNAi, which has relatively low penetrance. Our analysis also focused on expression changes as a function of CSR-1 22G RNA density, instead of treating the set of genes with homology to CSR-1 22G RNAs as a single entity and imposing a fixed threshold. Regardless of the precise reasons, our findings show that a substantial number of targets are tuned by CSR-1 catalytic activity, with 133 highly tuned targets (such as MCAK^{KLP-7}, CSR-1, and SPD-5; Table

S1), and lower amplitude tuning of a large proportion of germline-expressed targets. Tuning of major targets, such as MCAK^{KLP-7}, is essential, as elevated MCAK^{KLP-7} levels lead to severe phenotypes; the net effect of lower amplitude tuning of a large number of germline transcripts likely also contributes to embryo fitness. The fact that CSR-1 activity autoregulates its own expression is consistent with its role as a tissue-wide master regulator, by analogy with developmentally critical transcription factors that often employ autoregulation to control of their own levels (Crews and Pearson, 2009).

The fact that CSR-1-22G RNA complexes control target expression complicates interpretation of other proposed roles for the CSR-1-22G RNA pathway. We discuss a subset of these roles below but, more broadly, highlight the need to re-evaluate prior work in light of the results reported here.

Chromosome Organization and Segregation

Our initial motivation to study CSR-1 was based on its proposed role in chromosome/centromere organization (Claycomb et al., 2009). While our results confirm a centrally important role for the CSR-1-22G RNA pathway in chromosome segregation, they do not support a direct role for CSR-1-22G RNA complexes in patterning holocentric chromosome structure. The phenotypic differences between depletion of the histone mRNA stem-loop-binding factor CDL-1 and CSR-1 inhibition also suggest that a role in histone mRNA maturation does not account for the chromosome segregation defects associated with loss of CSR-1 activity. Instead, CSR-1 controls chromosome segregation in part, but not exclusively, via control of a key regulator of microtubule dynamics—the microtubule depolymerase MCAK^{KLP-7}.

P-Granule Assembly and Fertility

The CSR-1 slicing activity mutant exhibits the same phenotypic profile as loss of CSR-1 with two exceptions: the slicing mutant has a higher brood size than the null mutant and does not appear to disrupt perinuclear P granules in the germline, as reported previously for a *csr-1* mutant and *csr-1(RNA)* (Campbell and Updike, 2015; Claycomb et al., 2009). Recent work suggests that knockdown of *csr-1* or of P-granule components leads to inappropriate expression of spermatogenesis genes (Campbell and Updike, 2015). In the CSR-1 catalytic activity mutant, there was only a mild increase in mRNA levels of spermatogenesis genes (2,641 genes defined by Ortiz et al., 2014; the mean log₂foldchange for this gene set in CSR-1^{SIN} versus CSR-1^{WT} was 0.39 [1.3-fold]; the median was 0.32 [1.25-fold]; RPKM >1

Figure 6. Genome-wide Analysis Reveals Tuning Down of mRNA Levels by CSR-1 Catalytic Activity that Is Correlated with 22G RNA Density

- (A) Venn diagram showing the 11,220 genes that meet the RPKM >1 in N2 and transcript length >300 bp thresholds; 4,101 of these genes have homology to CSR-1-bound 22G RNAs in N2 hermaphrodites (>25 normalized reads; Claycomb et al., 2009).
- (B) Plot of the change in mRNA levels between CSR-1^{SIN} and CSR-1^{WT} versus the density of CSR-1 22G RNAs for the 4,101 genes with homologous CSR-1-bound 22G RNAs. 22G RNA density was calculated as the ratio of normalized reads to the transcript abundance (RPKM) in N2.
- (C) Box-whiskers plot (5th–95th percentile) of the change in mRNA levels between CSR-1^{SIN} and CSR-1^{WT} for gene sets of increasing 22G RNA density. Mean and median are indicated by red solid and black dashed lines, respectively. Each bin is significantly different from the prior bin; the indicated p values are from t tests. The same plot with outliers is shown in Figure S6C.
- (D) Venn diagram of gene sets; 4,101 genes have homologous CSR-1-bound 22G RNAs. 2,101 genes are germline-enriched, based on prior microarray analysis (Claycomb et al., 2009). 436 of the germline-enriched genes do not overlap with the 4,101 CSR-1 22G RNA homology gene set.
- (E) Box-whiskers plot (5th–95th percentile) of the change in mRNA levels between CSR-1^{SIN} and CSR-1^{WT} for the indicated gene sets. The mean and median are indicated by black solid and black dashed lines, respectively. The indicated p values are from t tests. See also Figure S6D.
- (F) 344 genes exhibit >2-fold, significant ($p_{adj} < 0.05$) increase in mRNA levels in CSR-1^{SIN} relative to CSR-1^{WT}. Of the 344 genes, 133 overlap with the CSR-1 22G RNA gene set (green); the genes that do not overlap (gray) are expressed at significantly lower levels than the ones that do (see Figure S6E; Table S1). See also Figure S6 and Tables S1 and S2.

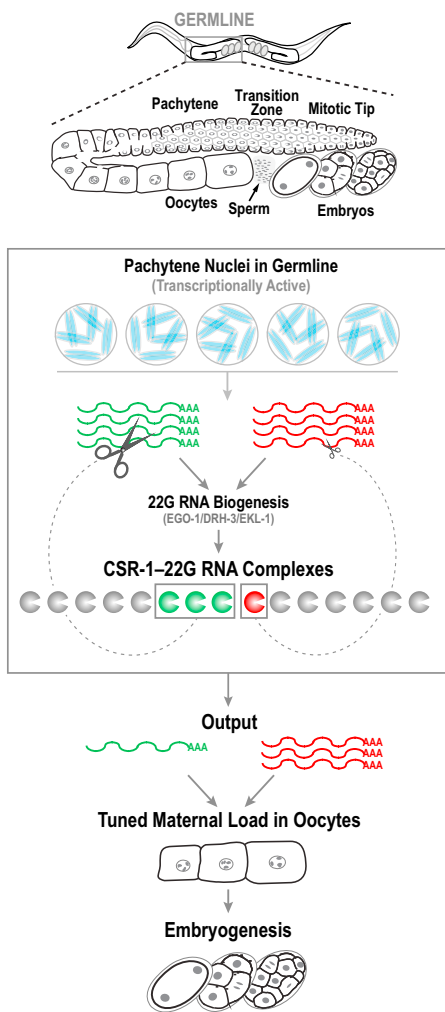


Figure 7. A Single Catalytic Argonaute Tunes Maternal Load Composition to Support Early Embryogenesis

The cartoon shows two mRNAs derived from transcriptionally active pachytene nuclei, one of which (green) is more prominently represented than the other (red) in the pool of CSR-1-22G RNA complexes. CSR-1 slicing tunes the mRNA levels guided by the proportional representation in the ensemble of CSR-1-22G RNA complexes to generate an output that supports early embryogenesis.

in N2 filter was not imposed as these genes are normally repressed in gravid N2 worms). A non-catalytic role of CSR-1 in a different process, such as translational repression in the mitotic region of the germline, where it acts together with the PUF domain protein FBF-1 (Friend et al., 2012), may also account for the brood size difference.

Self versus Non-self

Mating-based assays analyzing transgene silencing/activation, in conjunction with genomic analysis of small RNA pools, have revealed pathways acting in the germline to define self versus non-self (Ashe et al., 2012; Lee et al., 2012; Seth et al., 2013; Shirayama et al., 2012). The Piwi family Argonaute PRG-1, together with its associated 21U RNAs, initiates recognition of non-self genes and, via the action of the EGO-1/EKL-1/DRH-3

RNA-dependent RNA polymerase complex, triggers heritable WAGO-22G RNA-mediated silencing of foreign genes (Ashe et al., 2012; Lee et al., 2012; Shirayama et al., 2012). Imperfect homology to 21U RNAs, coded in vast numbers (~30,000 loci) in the genome, triggers 22G RNA generation and loading into the WAGO pathway. Self genes must be resistant to this non-self silencing pathway, and it has been proposed that CSR-1-22G RNA complexes protect self genes, potentially by acting on chromatin (Seth et al., 2013; Wedeles et al., 2013). How self gene-associated 22G RNAs are loaded into CSR-1 is not known. It is interesting to speculate whether the CSR-1-22G RNA pathway evolved to optimize maternal load by tuning levels of germline-expressed genes essential for fitness and then became co-opted to define self or vice versa.

Optimization of Maternal Load Composition by a Small RNA-Argonaute Pathway

Small RNA pathways have been long appreciated as being important for germline development and function. Here, we show that a slicing Argonaute-endogenous small RNA pathway comprised of CSR-1-22G RNAs controls target expression to generate oocytes capable of supporting early *C. elegans* embryogenesis. *csr-1* mutant males exhibit only modestly reduced fertility (Conine et al., 2013), highlighting a greater importance of this control mechanism in the oogenic germline. CSR-1 action in the oogenic germline is guided by 22G RNA cofactors generated by the RNA-dependent RNA polymerase (RdRP) EGO-1 (Figure 7), which presumably employs transcripts generated by meiotic pachytene nuclei (Lerner and Goldstein, 1988) as substrates. While RdRPs are thought to have been present in the ancestor to all eukaryotes and are present in fungi, plants, nematodes, and other metazoans, they have been lost in several animal groups, including vertebrates and insects (Zong et al., 2009). Despite loss of RdRPs, vertebrates have maintained one catalytically active Argonaute, Ago2. In mouse oocytes, Ago2 acts in concert with endogenous siRNAs—some of which are derived from Dicer processing of dsRNA intermediates containing pseudogene transcripts—to tune the expression of protein-coding transcripts (Stein et al., 2015; Tam et al., 2008; Watanabe et al., 2008). Ago2 slicing activity is dispensable for oocyte formation and growth but is required for oocyte spindle assembly, meiotic divisions, and female fertility (Stein et al., 2015). As with *csr-1* mutant males in *C. elegans*, Ago2 removal does not result in male infertility, highlighting that the essential role for Ago2 catalytic activity-based tuning is in the female germline. Intriguingly, plants harbor multiple RdRPs and also employ catalytic Argonautes to control female gamete development (Nonomura et al., 2007; Olmedo-Monfil et al., 2010). Thus, while the specific catalytic Argonautes and their small RNA cofactor generation mechanisms do not share a common ancestry, the use of catalytic Argonautes in the generation of female gametes capable of supporting early embryogenesis appears widespread.

We speculate that one reason for the existence of such a post-transcriptional layer of regulation is the special nature of germline chromatin, where tight suppression of somatic expression to maintain pluripotency may limit the precision of transcriptional control. For example, experiments in *C. elegans* assessing the

effects of ectopic expression of neuronal type-specifying master transcriptional regulators have shown that the germline is refractory to fate changes unless global chromatin states are altered (Tursun et al., 2011). Thus, the female germline appears to have adapted small RNA-catalytic Argonaute pathways to act post-transcriptionally in order to optimize maternal load composition. A post-transcriptional layer of control in the germline may also leave open promoter-based regulation of target genes in differentiated cells, where the amount of the gene product required may be different from what is needed in early embryogenesis. For example, MCAK^{KLP-7} controls dynamics of microtubule arrays in rapidly dividing cells of the early *C. elegans* embryo but also regulates microtubule dynamics in neurons (Ghosh-Roy et al., 2012), where a different amount of MCAK^{KLP-7} activity may be required.

As CSR-1 slicing is guided by 22G RNA density, nucleotide changes in the transcript sequence that influence 22G RNA generation can be translated via CSR-1 slicing activity into changes in expression level. Thus, we speculate that small RNA-catalytic Argonaute-mediated post-transcriptional control enables evolutionary optimization of the relative representation of the array of proteins and RNAs in the maternal load by exerting selective pressure on randomly occurring sequence changes that modulate small RNA generation and, consequently, stoichiometry in the maternal load. The major question raised by our findings is precisely how 22G RNA biogenesis by the EGO-1 RNA-dependent RNA polymerase complex is controlled. Understanding the rules that govern 22G RNA synthesis may be facilitated by the development of reporters for CSR-1 targets, such as MCAK^{KLP-7}.

EXPERIMENTAL PROCEDURES

C. elegans strains (Table S2) were maintained using standard methods. A transposon-based strategy (Frøkjaer-Jensen et al., 2008) was used to insert *csr-1* transgenes in single copy at a defined genomic location on chromosome 2. All *csr-1* transgenes included 2,168 bp upstream of the start codon for isoform a and 1,048 bp downstream of the stop codon; a segment (Figure S3A) was modified to preserve coding information but alter nucleotide sequence, to make transgene-encoded products resistant to a dsRNA that depletes endogenous CSR-1. RNAi (conducted by injection of dsRNAs; Table S3), worm dissection, and embryo mounting for live imaging were performed as previously described (Cheeseman et al., 2004). For the immunoblotting, qPCR, and mRNA-Seq analysis, first-generation homozygotes for the untagged *csr-1* transgene insertion (either WT or S1N) and the *csr-1(tm892)* null mutation (Figure S2A) were picked for analysis. Transgene insertions on chromosome 2 were first homozygosed and maintained in balanced *csr-1(tm892)* heterozygotes (the *csr-1* locus is on chromosome 4; transgene insertions are on chromosome 2). Homozygous *csr-1(tm892)* worms were isolated from balanced heterozygous *csr-1(tm892)* mothers based on their differential motility due to a balancer-associated *unc* mutation. For immunoblotting, equal numbers of worms of indicated genotypes were picked, washed in buffer, and boiled with intermittent sonication in sample buffer. For analysis of mRNA levels of selected genes and mRNA-Seq, total RNA from equal number of worms was extracted using Trizol. For analysis of mRNA levels, mRNA was isolated from total RNA and reverse transcribed into cDNA, and qPCR analysis was performed using the primers listed in Table S4. For mRNA-Seq, libraries were generated using Illumina TruSeq Stranded mRNA Sample Prep Kit, multiplexed, and sequenced with 50-bp single-end reads to a depth of ~40 million reads per sample. Details on the imaging conditions used and on the quantitative analysis of fluorescence, immunoblotting, qPCR, and mRNA-Seq data are in the Supplemental Experimental Procedures.

ACCESSION NUMBERS

The accession number for the mRNA-Seq data reported in this paper is GEO:GSE75128.

SUPPLEMENTAL INFORMATION

Supplemental Information includes Supplemental Experimental Procedures, six figures, and five tables and can be found with this article online at <http://dx.doi.org/10.1016/j.cell.2016.02.040>.

AUTHOR CONTRIBUTIONS

A.G.-G. and A.D. initiated the project; A.G.-G. performed the majority of experiments with help from S.W., R.G., and K.O. on imaging-based phenotypic analysis and immunoblotting; S.W., S.S., and G.W.Y. performed analysis of sequencing data with feedback from A.D.; and A.G.-G., S.W., A.D., and K.O. prepared the manuscript, with input from all of the other authors.

ACKNOWLEDGMENTS

We thank Amy Pasquinelli, Andreas Rechtsteiner, James Broughton, and the members of the A.D. and K.O. labs for helpful discussions and Kristen Jepsen and the UCSD Institute for Genomic Medicine Genomics Center for help with sequencing. This work was supported by an NIH grant (GM074215) (to A.D.). A.G.-G. was supported by an EMBO Long-Term Fellowship (ALTF 251-2012). G.W.Y. and S.S. are supported by grants from the NIH (HG004659, MH107369, and NS075449). A.D. and K.O. receive salary and other support from the Ludwig Institute for Cancer Research.

Received: November 17, 2015

Revised: January 20, 2016

Accepted: February 18, 2016

Published: March 24, 2016

REFERENCES

- Aoki, K., Moriguchi, H., Yoshioka, T., Okawa, K., and Tabara, H. (2007). In vitro analyses of the production and activity of secondary small interfering RNAs in *C. elegans*. *EMBO J.* **26**, 5007–5019.
- Ashe, A., Sapetschnig, A., Weick, E.M., Mitchell, J., Bagijn, M.P., Cording, A.C., Doebley, A.L., Goldstein, L.D., Lehrbach, N.J., Le Pen, J., et al. (2012). piRNAs can trigger a multigenerational epigenetic memory in the germline of *C. elegans*. *Cell* **150**, 88–99.
- Avgousti, D.C., Palani, S., Sherman, Y., and Grishok, A. (2012). CSR-1 RNAi pathway positively regulates histone expression in *C. elegans*. *EMBO J.* **31**, 3821–3832.
- Batista, P.J., Ruby, J.G., Claycomb, J.M., Chiang, R., Fahlgren, N., Kasschau, K.D., Chaves, D.A., Gu, W., Vasale, J.J., Duan, S., et al. (2008). PRG-1 and 21U-RNAs interact to form the piRNA complex required for fertility in *C. elegans*. *Mol. Cell* **31**, 67–78.
- Billi, A.C., Fischer, S.E., and Kim, J.K. (2014). Endogenous RNAi pathways in *C. elegans*. In WormBook, the *C. elegans* research community, eds. doi/<http://dx.doi.org/10.1895/wormbook.1.7.1>, <http://www.wormbook.org>.
- Buckley, B.A., Burkhart, K.B., Gu, S.G., Spracklin, G., Kershner, A., Fritz, H., Kimble, J., Fire, A., and Kennedy, S. (2012). A nuclear Argonaute promotes multigenerational epigenetic inheritance and germline immortality. *Nature* **489**, 447–451.
- Campbell, A.C., and Updike, D.L. (2015). CSR-1 and P granules suppress sperm-specific transcription in the *C. elegans* germline. *Development* **142**, 1745–1755.
- Carmell, M.A., Xuan, Z., Zhang, M.Q., and Hannon, G.J. (2002). The Argonaute family: tentacles that reach into RNAi, developmental control, stem cell maintenance, and tumorigenesis. *Genes Dev.* **16**, 2733–2742.

- Cecere, G., Hoersch, S., O'Keeffe, S., Sachidanandam, R., and Grishok, A. (2014). Global effects of the CSR-1 RNA interference pathway on the transcriptional landscape. *Nat. Struct. Mol. Biol.* 21, 358–365.
- Cheeseman, I.M., Niessen, S., Anderson, S., Hyndman, F., Yates, J.R., 3rd, Oegema, K., and Desai, A. (2004). A conserved protein network controls assembly of the outer kinetochore and its ability to sustain tension. *Genes Dev.* 18, 2255–2268.
- Claycomb, J.M., Batista, P.J., Pang, K.M., Gu, W., Vasale, J.J., van Wolfswinkel, J.C., Chaves, D.A., Shirayama, M., Mitani, S., Ketting, R.F., et al. (2009). The Argonaute CSR-1 and its 22G-RNA cofactors are required for holocentric chromosome segregation. *Cell* 139, 123–134.
- Conine, C.C., Moresco, J.J., Gu, W., Shirayama, M., Conte, D., Jr., Yates, J.R., 3rd, and Mello, C.C. (2013). Argonautes promote male fertility and provide a paternal memory of germline gene expression in *C. elegans*. *Cell* 155, 1532–1544.
- Crews, S.T., and Pearson, J.C. (2009). Transcriptional autoregulation in development. *Curr. Biol.* 19, R241–R246.
- Das, P.P., Bagijn, M.P., Goldstein, L.D., Woolford, J.R., Lehrbach, N.J., Sa-petschnig, A., Buhecha, H.R., Gilchrist, M.J., Howe, K.L., Stark, R., et al. (2008). Piwi and piRNAs act upstream of an endogenous siRNA pathway to suppress Tc3 transposon mobility in the *Caenorhabditis elegans* germline. *Mol. Cell* 31, 79–90.
- Decker, M., Jaensch, S., Pozniakovsky, A., Zinke, A., O'Connell, K.F., Zachariae, W., Myers, E., and Hyman, A.A. (2011). Limiting amounts of centrosome material set centrosome size in *C. elegans* embryos. *Curr. Biol.* 21, 1259–1267.
- Desai, A., Verma, S., Mitchison, T.J., and Walczak, C.E. (1999). Kin I kinesins are microtubule-destabilizing enzymes. *Cell* 96, 69–78.
- Friend, K., Campbell, Z.T., Cooke, A., Kroll-Conner, P., Wickens, M.P., and Kimble, J. (2012). A conserved PUF-Ago-eEF1A complex attenuates translation elongation. *Nat. Struct. Mol. Biol.* 19, 176–183.
- Frokjaer-Jensen, C., Davis, M.W., Hopkins, C.E., Newman, B.J., Thummel, J.M., Olesen, S.P., Grunnet, M., and Jorgensen, E.M. (2008). Single-copy insertion of transgenes in *Caenorhabditis elegans*. *Nat. Genet.* 40, 1375–1383.
- Gassmann, R., Rechtsteiner, A., Yuen, K.W., Muroyama, A., Egelhofer, T., Gaydos, L., Barron, F., Maddox, P., Essex, A., Monen, J., et al. (2012). An inverse relationship to germline transcription defines centromeric chromatin in *C. elegans*. *Nature* 484, 534–537.
- Ghosh-Roy, A., Goncharov, A., Jin, Y., and Chisholm, A.D. (2012). Kinesin-13 and tubulin posttranslational modifications regulate microtubule growth in axon regeneration. *Dev. Cell* 23, 716–728.
- Grishok, A. (2013). Biology and mechanisms of short RNAs in *Caenorhabditis elegans*. *Adv. Genet.* 83, 1–69.
- Gu, W., Shirayama, M., Conte, D., Jr., Vasale, J., Batista, P.J., Claycomb, J.M., Moresco, J.J., Youngman, E.M., Keys, J., Stoltz, M.J., et al. (2009). Distinct argonaute-mediated 22G-RNA pathways direct genome surveillance in the *C. elegans* germline. *Mol. Cell* 36, 231–244.
- Hamill, D.R., Severson, A.F., Carter, J.C., and Bowerman, B. (2002). Centrosome maturation and mitotic spindle assembly in *C. elegans* require SPD-5, a protein with multiple coiled-coil domains. *Dev. Cell* 3, 673–684.
- Kuhn, C.D., and Joshua-Tor, L. (2013). Eukaryotic Argonautes come into focus. *Trends Biochem. Sci.* 38, 263–271.
- Lee, H.C., Gu, W., Shirayama, M., Youngman, E., Conte, D., Jr., and Mello, C.C. (2012). *C. elegans* piRNAs mediate the genome-wide surveillance of germline transcripts. *Cell* 150, 78–87.
- Lerner, K., and Goldstein, P. (1988). Electron microscopic autoradiographic analysis: evidence of RNA transcription along pachytene chromosomes of *rad-4*, *him-4* and wild-type *Caenorhabditis elegans*. *Cytobios* 55, 51–61.
- Maniar, J.M., and Fire, A.Z. (2011). EGO-1, a *C. elegans* RdRP, modulates gene expression via production of mRNA-templated short antisense RNAs. *Curr. Biol.* 21, 449–459.
- Nonomura, K., Morohoshi, A., Nakano, M., Eiguchi, M., Miyao, A., Hirochika, H., and Kurata, N. (2007). A germ cell specific gene of the ARGONAUTE family is essential for the progression of premeiotic mitosis and meiosis during sporogenesis in rice. *Plant Cell* 19, 2583–2594.
- Olmedo-Monfil, V., Durán-Figueroa, N., Arteaga-Vázquez, M., Demesa-Arévalo, E., Autran, D., Grimanelli, D., Slotkin, R.K., Martienssen, R.A., and Vielle-Calzada, J.P. (2010). Control of female gamete formation by a small RNA pathway in *Arabidopsis*. *Nature* 464, 628–632.
- Ortiz, M.A., Noble, D., Sorokin, E.P., and Kimble, J. (2014). A new dataset of spermatogenic vs. oogenic transcriptomes in the nematode *Caenorhabditis elegans*. *G3 (Bethesda)* 4, 1765–1772.
- Reinke, V., Gil, I.S., Ward, S., and Kazmer, K. (2004). Genome-wide germline-enriched and sex-biased expression profiles in *Caenorhabditis elegans*. *Development* 131, 311–323.
- Seth, M., Shirayama, M., Gu, W., Ishidate, T., Conte, D., Jr., and Mello, C.C. (2013). The *C. elegans* CSR-1 argonaute pathway counteracts epigenetic silencing to promote germline gene expression. *Dev. Cell* 27, 656–663.
- Shirayama, M., Seth, M., Lee, H.C., Gu, W., Ishidate, T., Conte, D., Jr., and Mello, C.C. (2012). piRNAs initiate an epigenetic memory of nonself RNA in the *C. elegans* germline. *Cell* 150, 65–77.
- Stein, P., Rozhkov, N.V., Li, F., Cárdenas, F.L., Davydenko, O., Vandivier, L.E., Gregory, B.D., Hannon, G.J., and Schultz, R.M. (2015). Essential Role for endogenous siRNAs during meiosis in mouse oocytes. *PLoS Genet.* 11, e1005013.
- Swarts, D.C., Makarova, K., Wang, Y., Nakanishi, K., Ketting, R.F., Koonin, E.V., Patel, D.J., and van der Oost, J. (2014). The evolutionary journey of Argonaute proteins. *Nat. Struct. Mol. Biol.* 21, 743–753.
- Tabara, H., Sarkissian, M., Kelly, W.G., Fleenor, J., Grishok, A., Timmons, L., Fire, A., and Mello, C.C. (1999). The rde-1 gene, RNA interference, and transposon silencing in *C. elegans*. *Cell* 99, 123–132.
- Tam, O.H., Aravin, A.A., Stein, P., Girard, A., Murchison, E.P., Cheloufi, S., Hodges, E., Anger, M., Sachidanandam, R., Schultz, R.M., and Hannon, G.J. (2008). Pseudogene-derived small interfering RNAs regulate gene expression in mouse oocytes. *Nature* 453, 534–538.
- Tursun, B., Patel, T., Kratsios, P., and Hobert, O. (2011). Direct conversion of *C. elegans* germ cells into specific neuron types. *Science* 331, 304–308.
- Updike, D.L., and Strome, S. (2009). A genomewide RNAi screen for genes that affect the stability, distribution and function of P granules in *Caenorhabditis elegans*. *Genetics* 183, 1397–1419.
- Wang, S., Wu, D., Quintin, S., Green, R.A., Cheerambathur, D.K., Ochoa, S.D., Desai, A., and Oegema, K. (2015). NOCA-1 functions with γ -tubulin and in parallel to Patronin to assemble non-centrosomal microtubule arrays in *C. elegans*. *eLife* 4, e08649.
- Watanabe, T., Totoki, Y., Toyoda, A., Kaneda, M., Kuramochi-Miyagawa, S., Obata, Y., Chiba, H., Kohara, Y., Kono, T., Nakano, T., et al. (2008). Endogenous siRNAs from naturally formed dsRNAs regulate transcripts in mouse oocytes. *Nature* 453, 539–543.
- Wedeles, C.J., Wu, M.Z., and Claycomb, J.M. (2013). Protection of germline gene expression by the *C. elegans* Argonaute CSR-1. *Dev. Cell* 27, 664–671.
- Woodruff, J.B., Wueseke, O., Viscardi, V., Mahamid, J., Ochoa, S.D., Bunkerborg, J., Widlund, P.O., Pozniakovsky, A., Zanin, E., Bahmanyar, S., et al. (2015). Centrosomes. Regulated assembly of a supramolecular centrosome scaffold in vitro. *Science* 348, 808–812.
- Yigit, E., Batista, P.J., Bei, Y., Pang, K.M., Chen, C.C., Tolia, N.H., Joshua-Tor, L., Mitani, S., Simard, M.J., and Mello, C.C. (2006). Analysis of the *C. elegans* Argonaute family reveals that distinct Argonautes act sequentially during RNAi. *Cell* 127, 747–757.
- Zong, J., Yao, X., Yin, J., Zhang, D., and Ma, H. (2009). Evolution of the RNA-dependent RNA polymerase (RdRP) genes: duplications and possible losses before and after the divergence of major eukaryotic groups. *Gene* 447, 29–39.